NASA TECHNICAL MEMORANDUM

NASA TM X-1364

NASA TM X-1364



# EFFECT OF SIMULATED BEARING COOLANT INJECTION ON THE PERFORMANCE OF A TWO-STAGE, VELOCITY-COMPOUNDED TURBOPUMP DRIVE TURBINE

*by Roy G. Stabe, John F. Kline, and Edward H. Gibbs*

*Lewis Research Center*

*Cleveland, Ohio*

NATIONAL AERONAUTICS AND SPACE ADMINISTRATION • WASHINGTON, D. C. • APRIL 1967

NASA TM X-1364

# EFFECT OF SIMULATED BEARING COOLANT INJECTION ON THE PERFORMANCE OF A TWO-STAGE, VELOCITY-COMPOUNDED TURBOPUMP DRIVE TURBINE

By Roy G. Stabe, John F. Kline, and Edward H. Gibbs

Lewis Research Center
Cleveland, Ohio

NATIONAL AERONAUTICS AND SPACE ADMINISTRATION

For sale by the Clearinghouse for Federal Scientific and Technical Information
Springfield, Virginia 22151 – CFSTI price $3.00

# EFFECT OF SIMULATED BEARING COOLANT INJECTION ON THE PERFORMANCE OF A TWO-STAGE, VELOCITY-COMPOUNDED TURBOPUMP DRIVE TURBINE

by Roy G. Stabe, John F. Kline, and Edward H. Gibbs
Lewis Research Center

## SUMMARY

The effect of simulated bearing coolant injection on the performance of a two-stage, velocity-compounded turbopump drive turbine was investigated experimentally at the NASA Lewis Research Center. The 0.646-scale-model turbine used for the cold-air performance evaluation of the M-1 fuel turbine was modified to provide for the introduction of measured amounts of secondary air into the space between the nozzle and the first-stage rotor to simulate bearing coolant injection. The secondary air mixes with the primary flow, also air, at the nozzle exit and proceeds through the remaining blade rows as part of the working fluid. Performance data were taken for one- and two-stage turbine configurations over a range of operating conditions and for four secondary flow rates of 0, 3, 7, and 10 percent of the primary flow.

At design equivalent speed and pressure ratio, the two-stage turbine equivalent specific work decreased from 29.7 Btu per pound of primary flow at zero secondary flow to 27.0 Btu per pound of primary flow at a secondary flow rate of 10 percent of primary flow, with a corresponding decrease in static efficiency from 0.650 to 0.593.

Each increment of secondary flow resulted in substantial increases in interstage static pressures. The largest increase occurred at the exit of the converging-diverging nozzle. The reaction of the first stage increased markedly with each increment of secondary flow addition, which was also true, to a lesser extent, of the second stage. Both stages were forced farther off design operation as the secondary flow rate increased. First-stage equivalent specific work decreased from 21.3 Btu per pound of primary flow at zero secondary flow to 17.3 Btu per pound of primary flow at a secondary flow rate of 10 percent of primary flow. First-stage losses were relatively constant over the range of secondary flow rates. The loss in work resulted primarily from decreased energy available to the first stage because of the pressure changes noted previously.

The energy available to the second stage increased with secondary flow rate. Some of this energy was converted to work. Second-stage equivalent specific work increased from 8.4 Btu per pound of primary flow at zero secondary flow to 9.7 Btu per pound at a secondary flow rate of 10 percent of primary flow. Second-stage losses, however, also increased, resulting in a further decrease in two-stage turbine work output as the secondary flow rate increased from 0 to 10 percent of primary flow.

# INTRODUCTION

Secondary fluid addition to the primary flow occurs in several turbine applications that include, for example, jet-engine turbine blade and disk cooling air, and rocket-engine turbopump bearing coolant (usually a cryogenic propellant) that is vented into the drive turbine casing. The introduction of a secondary fluid, perhaps with very different thermodynamic properties, into the primary flow stream would be expected to affect turbine performance. Performance changes may occur through the work required to pump the secondary fluid into the primary flow stream, through differences in thermodynamic properties, through energy and momentum exchange, and through changes in turbine pressure distribution resulting from additional flow. The effect of secondary fluid addition on the turbine internal flow processes depends on the properties and the amount of secondary fluid injected, the method of injection, and the turbine design. For example, the effect of cooling air injected through slots in the blades of a jet-engine turbine could be quite different from the effect of injecting a cryogenic propellant, which had been used to cool the turbopump bearings, into the space between the nozzle and rotor disk of the turbopump drive turbine.

The effect of simulated bearing coolant injection on the performance of a two-stage, velocity-compounded turbopump drive turbine has been investigated experimentally at the NASA Lewis Research Center. The turbine used for this investigation was the 0.646-scale-model turbine used for the cold-air performance evaluation of the M-1 fuel turbine (refs. 1 and 2). The blading for this turbine was designed with no provision for a secondary fluid flow. For the subject program, the bearing housing of the scale-model turbine was modified to provide for the introduction of measured amounts of secondary air into the space between the nozzle and the first-stage rotor disk to simulate bearing coolant injection. The secondary air mixes with the primary flow, also air, at the nozzle exit and proceeds through the remaining blade rows as part of the working fluid. Performance data were taken for one- and two-stage turbine configurations over a range of operating conditions and for four secondary flow rates of 0, 3, 7, and 10 percent of primary flow.

Turbine performance in terms of static efficiency, equivalent specific work, and interstage static pressures are presented for the range of secondary flow rates covered in the investigation. The results of an analysis to determine the magnitude of the various turbine losses resulting from the secondary flow addition is also presented.

# SYMBOLS

$C_{vn}$ nozzle velocity coefficient, $\left(V/V_s\right)_3 = V_3 \Big/ \left\{2g_c J c_p T'_1 \left[1 - (p_3/p'_2)^{(\gamma-1)/\gamma}\right]\right\}^{1/2}$

$C_{wr}$ rotor velocity coefficient, $\left(W/W_s\right)_4 = W_4 \Big/ \left\{2g_c J c_p T_3'' \left[1 - (p_4/p_3'')^{(\gamma-1)/\gamma}\right]\right\}^{1/2}$

$c_p$ specific heat at constant pressure, Btu/(lb)($^oR$)

$g_c$ dimensional conversion constant, 32.17 ft-lb/lb-sec$^2$

h specific enthalpy, Btu/lb

$\Delta h'$ specific work, Btu/lb

$\Delta h_s$ ideal available energy, $\Delta h_s = c_p T_1' \left[1 - (p_{exit}/p_1')^{(\gamma-1)/\gamma}\right]$, Btu/lb

J mechanical equivalent of heat, 778 ft-lb/Btu

N speed, rpm

p absolute pressure, lb/in.$^2$

$\mathscr{R}_s$ isentropic first-stage reaction, $\left(h_3 - h_4\right)_s \Big/ \left(h_2' - h_4\right)_s$

$= (p_3/p_2')^{(\gamma-1)/\gamma} \left[1 - (p_4/p_3)^{(\gamma-1)/\gamma}\right] \Big/ \left[1 - (p_4/p_2')^{(\gamma-1)/\gamma}\right]$

T temperature, $^oR$

U blade speed, ft/sec

V absolute velocity, ft/sec

W velocity relative to rotor blade, ft/sec

w weight flow, lb/sec

Y ratio of secondary to primary flow rates

$\alpha$ absolute flow angle, degrees from axial

$\beta$ relative flow angle, degrees from axial

$\gamma$ ratio of specific heats

$\delta$ ratio of inlet total pressure to NACA standard atmosphere pressure, $p_1'/14.696$

$\epsilon$ gamma correction function, $[0.74/\gamma][(\gamma + 1)/2]^{\gamma/(\gamma-1)}$

$\eta$ static efficiency based on total to static pressure ratio, $\Delta h'/\Delta h_s$

$\sqrt{\theta_{cr}}$ ratio of inlet critical velocity to critical velocity at NACA standard atmosphere, $V_{cr,1}/1019.46$

$\nu$ blade-jet speed ratio, $U_m/(2g_c J \Delta h_s)^{1/2}$

Subscripts:

cr conditions corresponding to those at Mach number of 1

exit rotor exit; station 4 (first stage) or station 6 (two stage)

| | |
|---|---|
| h | blade-hub section |
| m | blade-mean section |
| s | ideal or isentropic process |
| t | blade-tip section |
| 1, 2, 3, 4, 5, 6 | measuring station, see fig. 4 |

Superscripts:

| | |
|---|---|
| - | average value |
| ' | absolute total state condition |
| '' | total state condition relative to rotor |

## APPARATUS AND PROCEDURE

The scale-model turbine and cold-air test facility used for this investigation are described in reference 1. The test turbine, which is a two-stage, velocity-compounded machine with a mean diameter of 14.963 inches, is shown in figure 1 with part of the casing removed. The nozzle is convergent-divergent with an exit- to throat-area ratio of 1.172. Mean-diameter velocity diagrams for zero secondary flow at design equivalent speed and pressure ratio, computed from the performance data of reference 1, are shown in figure 2. Nozzle-exit and first-stage rotor-inlet relative velocities are supersonic. Performance data of reference 1 also indicate that the first-stage rotor is choked at the exit section. The two-stage equivalent specific work is 29.7 Btu per pound, of which the first stage contributes 21.3 Btu per pound or 71.7 percent of the total.

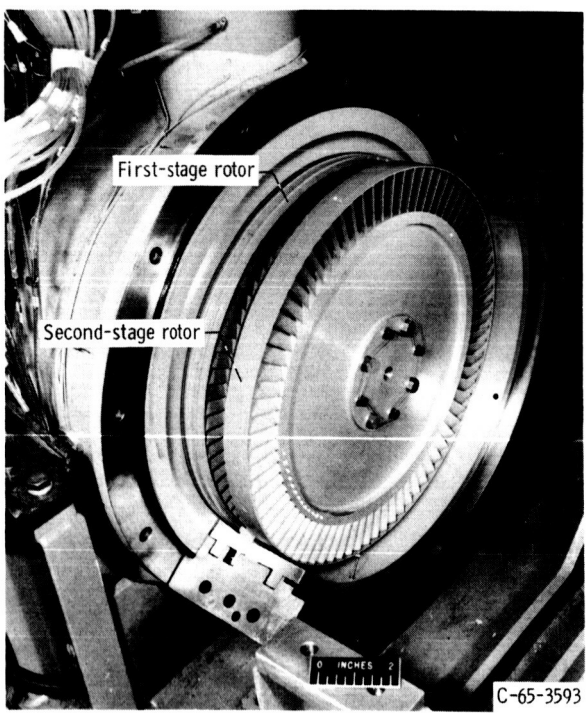


Figure 1. - Turbine assembly with half of casing removed.

The turbine bearing housing was altered to provide passages for the introduction of secondary air at low velocity into the space between the nozzle and the first-stage rotor disk. This space acted as a plenum to ensure uniform flow through the clearance space at the blade hub. A secondary air system was

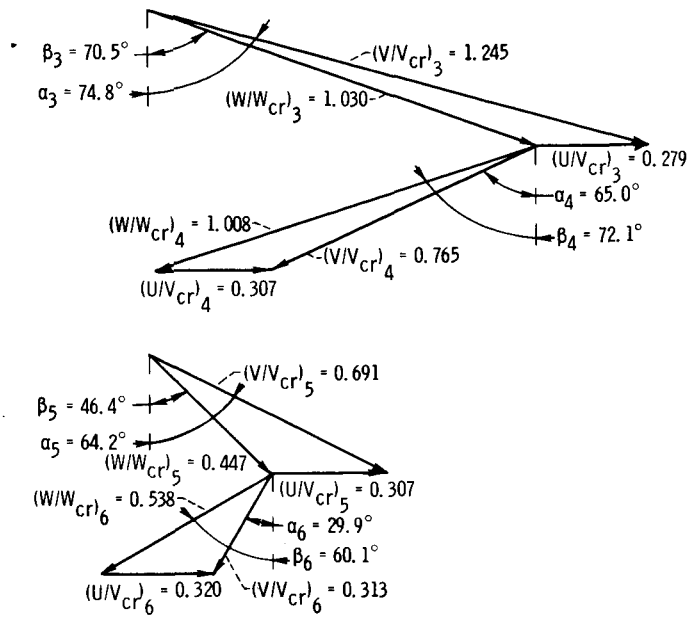


Figure 2. - Mean-diameter velocity diagrams obtained from experimental data. Design equivalent pressure ratio, $p'_1/p_{6,m}$, 4.97; design equivalent speed, $N/\sqrt{\theta_{cr}}$, 4361 rpm; zero secondary flow.

added to the facility to supply dry, ambient temperature air at any desired flow rate. A diagram and an overall view of the test facility are shown in figure 3.

The instrumentation in the turbine was identical to that used in the performance tests of reference 1. The axial and circumferential location of instrumentation in the test turbine is shown in figure 4. For tests of the first stage, the second-stage rotor and stator were removed. The stator was replaced with a fixture having similar inner and outer walls. Hub- and tip-wall static-pressure taps were provided at four circumferential locations at station 4 in this fixture.

For two-stage tests, two actuated combination (total-pressure - flow-angle) survey probes and one wedge-type static-pressure survey probe were located at the rotor exit, station 6. For first-stage tests, the combination probes were also located one blade chord downstream of the first-stage rotor.

The turbine was operated with dry primary air at $600^{\circ}$ R and 25 pounds per square inch absolute at the manifold inlet, station 1. The secondary air system was supplied with dry air at $540^{\circ}$ R. The two-stage turbine was operated at design equivalent pressure ratio (4.97) over a range of speeds from 60 to 100 percent of design equivalent speed (4361 rpm) for each of four secondary air flow rates: 0, 3, 7, and 10 percent of primary flow rate. Pressure, temperature, torque, and flow rate data were recorded at each turbine operating point. Radial surveys of rotor-exit flow angle, static pressure, and total pressure were made at design equivalent speed and pressure ratio for each of the four secondary flow rates. First-stage test procedure was similar; data were taken at design pressure ratio (4.25) and at a pressure ratio of 3.65 to permit interpolation of specific work to pressure ratios below design.

Primary and secondary air flow rates were measured with calibrated ASME orifice runs. Orifice inlet pressures were measured with calibrated precision Bourdon tube gages. All other pressures were recorded by photographing a bank of mercury manometers. Temperatures were read on an industrial self-balancing potentiometer. Turbine rotative speed was measured with an electronic counter in conjunction with a magnetic pickup and a 60-tooth, shaft-mounted gear. Turbine output power was absorbed by a

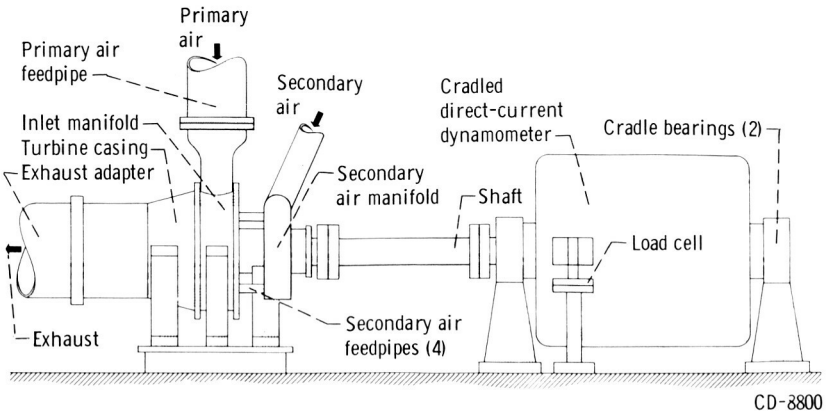


(a) Schematic diagram.

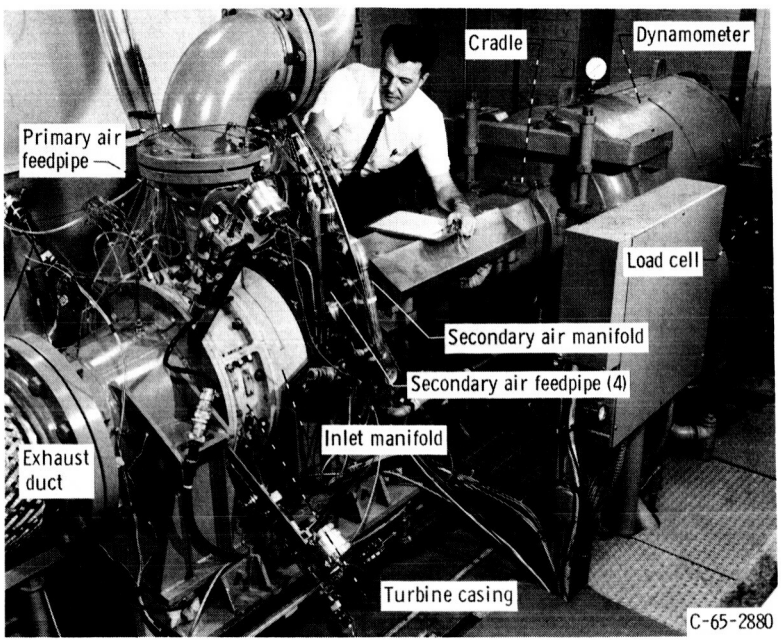


(b) Turbine installation.

Figure 3. - Turbine test facility.

cradled direct-current dynamometer. Torque was converted to pressure by a self-balancing pneumatic load cell, calibrated in place before and after each day's operation by deadweight loading of the dynamometer stator.

Turbine specific work $\Delta h'$ was calculated from speed, torque, and primary weight flow data. The secondary flow was not considered to be part of the working fluid for these calculations. The torque value used was the sum of the torque indicated by the dynamometer load cell and the test unit bearing and seal torque which had been determined separately.

The inlet or feedpipe total pressure was calculated from the average static pressure in the feedpipe (station 1), the flow area, the average inlet total temperature, and the

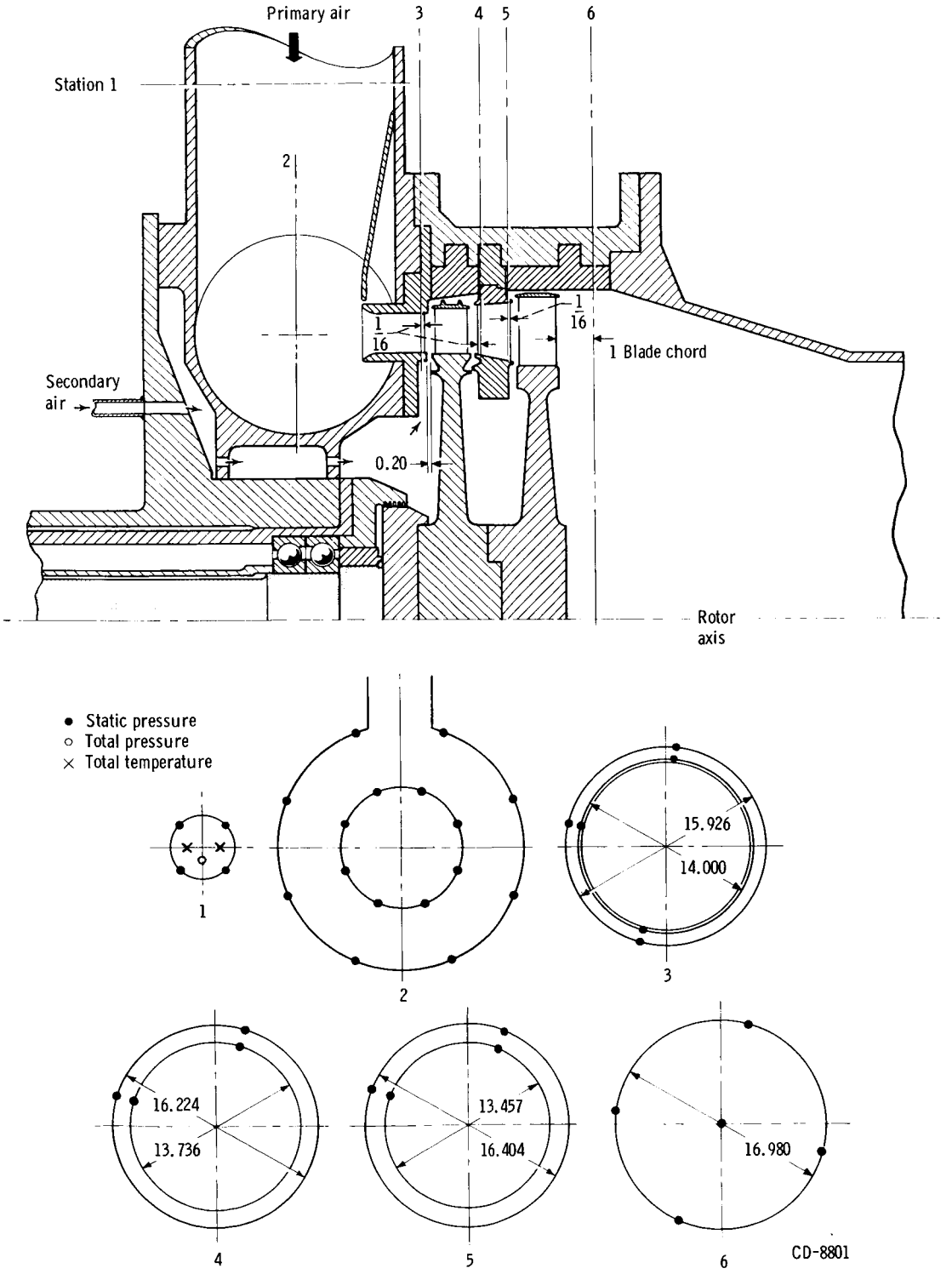


Figure 4. - Station nomenclature (all views looking upstream) and location of instrumentation. (All dimensions are in inches.)

weight flow. Two-stage turbine performance is based on the pressure ratio determined by the calculated inlet total pressure $p'_1$ and the measured static pressure $p_{6,m}$ at station 6. First-stage performance is based on the pressure ratio determined by the calculated inlet total pressure $p'_1$ and the average of the hub and tip average static pressures $\bar{p}_4$ measured at station 4.

## RESULTS AND DISCUSSION

The results of the cold-air investigation on the effect of simulated coolant injection on the performance of a two-stage, velocity-compounded turbine are presented in the following sections. Performance data are based on the primary weight flow. The secondary flow was treated as a perturbating parameter; that is, the dimensions of equivalent specific work $\Delta h'/\theta_{cr}$ are Btu per pound of primary flow. The first- and two-stage turbine tests were performed with the inlet manifold in place, and the performance data presented include losses attributable to the inlet manifold assembly.

The convergent-divergent nozzle choked at an inlet total- to nozzle-exit static-pressure ratio $p'_1/\bar{p}_3$ of 1.5. The performance data presented herein are all for nozzle pressure ratios greater than 1.5. The equivalent primary weight flow $\left(w\sqrt{\theta_{cr}}\epsilon\right)/\delta$ is therefore constant at the choking value of 2.88 pounds per second.

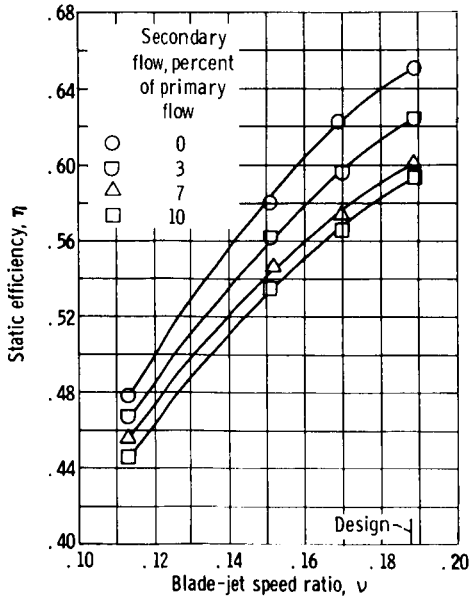


Figure 5. - Variation of two-stage static efficiency with blade-jet speed ratio and secondary flow rate at design equivalent pressure ratio.

### Two-Stage Turbine Performance

The two-stage turbine was operated at a design pressure ratio $p'_1/p_{6,m}$ of 4.97 and over a range of speeds from 60 to 100 percent of design equivalent speed for each of the secondary flow rates used in the investigation. Static efficiency as a function of blade-jet speed ratio and secondary flow rate is shown in figure 5. For each increment in secondary flow, there is a decrement in turbine performance over the range of blade-jet speed ratios covered in the investigation. At approximately design blade-jet speed ratio (0.188), the static efficiency decreases from 0.650 with no secondary flow to 0.624, 0.600, and 0.593 at secondary flow rates of 3, 7, and 10 percent of primary flow, respectively.

The axial distribution of hub- and tip-section

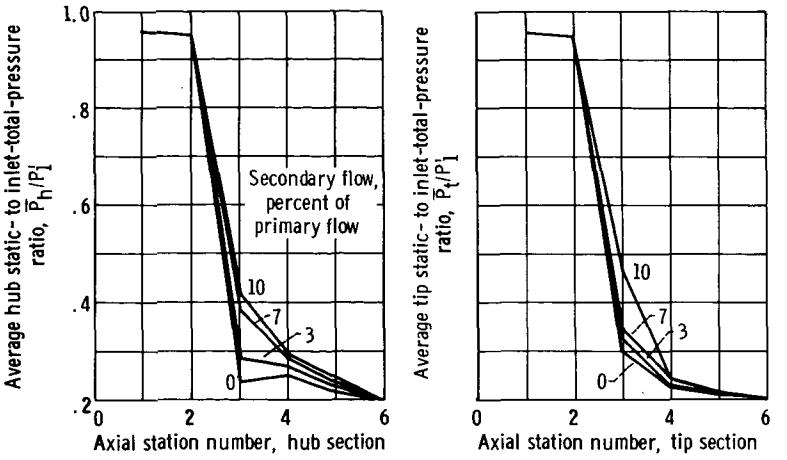


(a) Axial distribution of static pressure at hub and tip section.

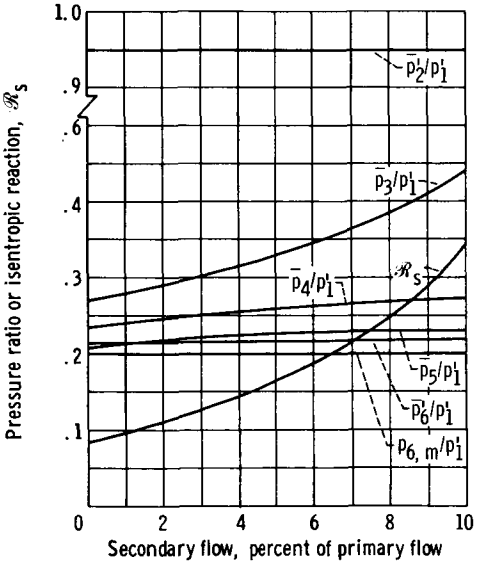


(b) Mean static pressures, average total pressures, and first-stage isentropic reaction.

Figure 6. - Variation of two-stage turbine pressure with secondary flow rate at design equivalent speed and pressure ratio.

static pressures for each of the secondary flow rates is shown in figure 6(a) (for design equivalent speed and pressure ratio). For each increment of secondary flow, there is a marked increase in first-stage static pressures and a smaller increase in second-stage static pressures. The hub-to-tip distribution of first-stage static pressures also changes considerably as the secondary flow rate increases. The static pressures in the feedpipe and manifold, stations 1 and 2, respectively, did not change as the nozzle was choked. A summary of the two-stage turbine pressures, as a function of the secondary flow rate, is shown in figure 6(b). The first-stage isentropic reaction $\mathscr{R}_s$ is also shown in this figure. The average nozzle-inlet to inlet total-pressure ratio $p'_2/p'_1$ was taken from reference 1.

The second-stage rotor-exit static- and total- to inlet total-pressure ratios ($p_{6,m}/p'_1$ and $\bar{p}'_6/p'_1$, respectively) are from the rotor-exit survey data. The nozzle-exit, second-stage stator inlet, and second-stage stator-exit static- to inlet total-pressure ratios $\bar{p}_3/p'_1$, $\bar{p}_4/p'_1$, and $\bar{p}_5/p'_1$ are the average value of the hub and tip static pressures measured at stations 3, 4, and 5, respectively. The nozzle-exit static pressure increased substantially with secondary flow. The first-stage exit static pressure also increased, but not as markedly. These changes have the effect of reducing the nozzle and first-stage pressure ratios, $p'_1/\bar{p}_3$ and $p'_1/\bar{p}_4$, respectively, and, consequently, the nozzle-exit velocity and energy available to the first stage. The static-pressure drop across the first-stage rotor also increased rapidly with secondary flow. This resulted in the first-stage changing from a nominal impulse stage at zero secondary flow to a stage with considerable reaction at the higher secondary flow rates. This change is indicated by the substantial increase in first-stage isentropic reaction $\mathscr{R}_s$ with secondary flow rate. In effect, each increment in secondary flow rate forced first-stage operation farther from design, which was also true, to a lesser extent, of the second stage. The pressure drop across both the second-stage stator and rotor, and consequently, the stage reaction, increased with secondary flow rate. The second-stage stator and rotor were also designed as nominal impulse blade rows; therefore, the second stage was also forced farther from design by each increment of secondary flow.

The large increase in first-stage static pressures and reaction with secondary flow rate increased the flow leakage through the clearance space around the first-stage rotor shroud. This leakage was calculated according to the method used in reference 2. The leakage flow increased from 4.9 percent of the flow at zero secondary flow to 7.0 percent of the combined primary and secondary flow at a secondary flow rate of 10.0 percent. There was a resultant increase in total flow through the first-stage rotor from 0.951 of the primary flow at zero secondary flow to 1.023 of the primary flow at a secondary flow rate of 10.0 percent. The first-stage rotor was choked, which necessitated higher pressures at the inlet (station 3) to provide for the larger flow. The increase in $\bar{p}_3/p'_1$ shown in figure 6(b), however, is apparently in excess of the increase required for the larger flow. The large increase in $\bar{p}_3/p'_1$ with secondary flow rate may have been the result of interaction between the supersonic primary flow at the nozzle exit with the secondary flow issuing radially outward through the clearance space between the nozzle and the first-stage rotor.

The second-stage rotor-exit total- to inlet total-pressure ratio $\bar{p}'_6/p'_1$ increases from 0.214 at zero secondary flow to 0.219 at a secondary flow rate of 10 percent of primary flow. This pressure was nearly uniform from hub to tip. The increase in pressure was also reflected in a small increase in the second-stage rotor-exit angle. The radial variation of pressure and angle were quite similar to those reported in reference 1; this was also true of the results of the first-stage rotor-exit surveys.

## First-Stage Performance

The first stage was operated at a constant pressure ratio $p'_1/\bar{p}_4$ of 4.25 (the first-stage operating pressure ratio for two-stage operation at zero secondary flow) for secondary flow rates of 0, 3, 7, and 10 percent of primary flow and over a range of speeds from 60 to 105 percent of design equivalent speed. First-stage static efficiency as a function of blade-jet speed ratio and secondary flow rate is shown in figure 7. For each increment in secondary flow, there is a decrement in first-stage performance similar to that seen for the two-stage turbine. At design blade-jet speed ratio (0.196), the static efficiency decreases from 0.506 with no secondary flow to 0.474, 0.446, and 0.430 at secondary flow rates of 3, 7, and 10 percent of primary flow, respectively. These decrements are larger than the corresponding changes noted for the two-stage turbine. The first stage was also tested at a pressure ratio $p'_1/\bar{p}_4$ of 3.65 (approximately the first-stage operating pressure ratio for two-stage operation at 10-percent secondary flow) at design equivalent speed and over the range of secondary flow rates. Reference 1 indicated that the first stage operates near limiting loading and that the equivalent specific work increases only a small amount as the pressure ratio increases from 3.65 to 4.25. Therefore, linear interpolation between these two pressure ratios was used to determine the first-stage equivalent specific work at the operating pressure ratios indicated in figure 6(b). The resulting first- and two-stage equivalent specific work $\Delta h'/\theta_{cr}$ are shown as functions of secondary flow rate in figure 8.

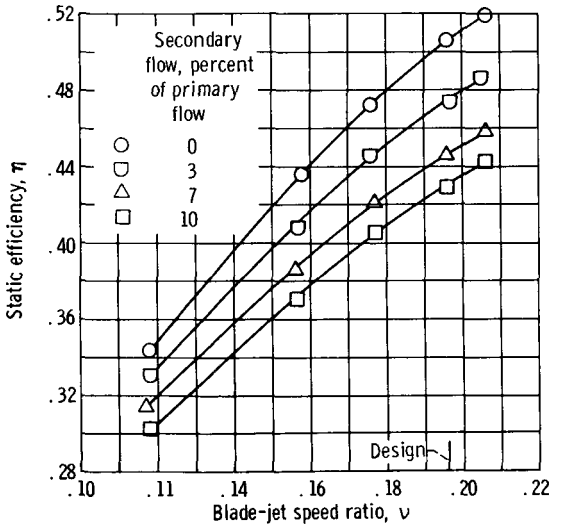


Figure 7. - Variation of first-stage static efficiency with blade-jet speed ratio and secondary flow rate at constant pressure ratio.

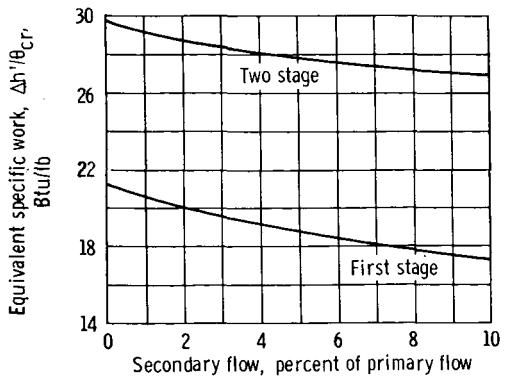


Figure 8. - Variation of first-stage and two-stage equivalent specific work with secondary flow rate at design equivalent speed speed and two-stage pressure ratio.

The equivalent specific work of the two-stage turbine decreased from 29.7 Btu per pound at zero secondary flow to 27.0 Btu per pound at a secondary flow rate of 10 percent of primary flow. The equivalent specific work of the first stage decreased from 21.3 Btu per pound at zero secondary flow to 17.3 Btu per pound at a secondary flow rate of 10 percent of primary flow. The second stage thus produces 8.4 Btu per pound at zero secondary flow and 9.7 Btu per pound at 10 percent secondary flow.

# ANALYSIS OF RESULTS

The effect of secondary air addition on the performance of a two-stage, velocity-compounded turbine was investigated, and the results presented thus far suggest that the first stage was largely responsible for the loss in turbine work associated with increasing secondary air flow rates. Accordingly, an analysis of the first-stage performance was undertaken to determine the magnitude of the various losses that occurred in the first stage, and by inference, the second-stage losses as well. The results of this analysis and a summary of the procedures used are presented in this section. The first-stage test data (weight flow, specific work, static pressures, mean diameter rotor-exit flow angle, and total pressures from the exit survey), which were for constant pressure ratio operation, were used to calculate first-stage velocity diagrams. Nozzle and rotor velocity coefficients $C_{vn}$ and $C_{wr}$ were then obtained from these diagrams and from the static-pressure data. The average value of nozzle-inlet total pressure from reference 1 $(\bar{p}'_2/p'_1 = 0.95)$ was also used in this calculation. The nozzle and rotor velocity coefficients were then used to determine the first-stage velocity diagrams for the pressures measured during two-stage operation (see fig. 6(b)). The calculation procedure is summarized as follows:

(1) The nozzle-exit velocity $V_3$ was calculated from the definition of the nozzle velocity coefficient $C_{vn}$ and from the value of $C_{vn}$ obtained from the previously determined constant-pressure-ratio velocity diagram at the corresponding secondary flow rate.

(2) The nozzle-exit flow angle $\alpha_3$ was determined from continuity.

(3) The first-stage rotor-exit relative velocity $W_4$ was calculated from the definition of the rotor velocity coefficient $C_{wr}$ and from the value of $C_{wr}$ obtained from the previously determined constant-pressure-ratio velocity diagram at the corresponding secondary flow rate.

(4) The first-stage rotor-exit relative flow angle $\beta_4$ was assumed to be the same as that of the previously determined constant-pressure-ratio diagram for the corresponding secondary flow rate.

(5) The resultant rotor-exit absolute flow angle $\alpha_4$ was then checked for agreement with continuity.

(6) Iteration of $C_{vn}$ and $C_{wr}$ was then repeated until satisfactory agreement with continuity and first-stage specific work was obtained (see fig. 8).

Velocity diagrams for secondary flow rates of 3, 7, and 10 percent of primary flow were thus determined. The resulting velocity coefficients, which differ very little from those obtained from the constant-pressure-ratio diagrams, are shown as functions of secondary flow rate in figure 9. There is relatively little change in the rotor velocity coefficient. The nozzle coefficient, however, decreases rapidly from 0.925 with no secondary flow and then levels off at 0.842 for secondary flow rates between 7 and 10 percent of primary

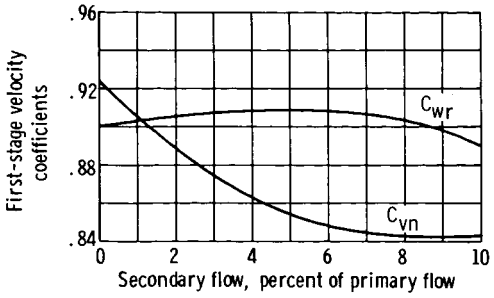


Figure 9. - Variation of first-stage nozzle and rotor velocity coefficients with secondary flow rate.

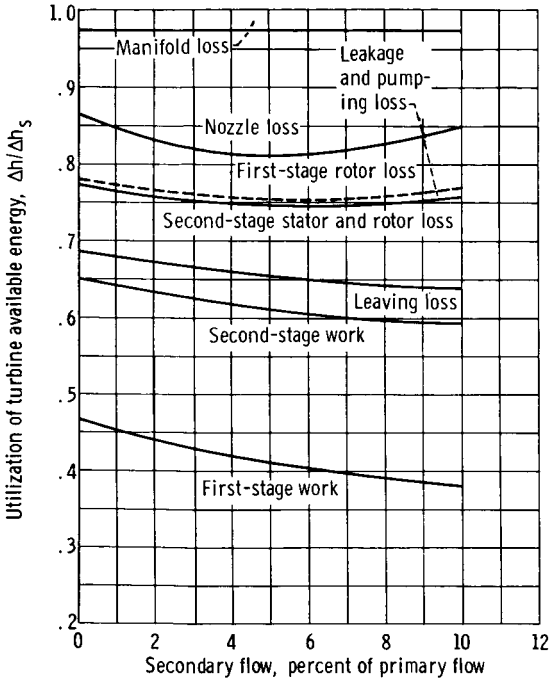


Figure 10. - Utilization of ideal available energy as function of secondary flow rate.

flow. The decrease in the nozzle velocity coefficient is a result of the rapidly changing nozzle pressure ratio, shown in figure 6, and this decrease is characteristic of convergent-divergent nozzle performance at off-design pressure ratios.

The velocity diagram and pressure data were then used to calculate the losses in available energy resulting from the nonisentropic processes that occurred in the manifold, nozzle, and first-stage rotor. Reference 3 was used for the calculation of pressures and temperatures, and reference 4 was used to determine the losses. The second-stage leaving loss was calculated from the rotor-exit total- and static-pressure survey data. The combined second-stage stator and rotor losses were taken as the difference between the ideal energy available to the two-stage turbine and the sum of the first- and second-stage work and manifold, nozzle, first-stage rotor, and leaving loss.

The utilization of energy, the ratio of work or loss to the ideal available energy, for the two-stage turbine over the range of secondary flow rates investigated is shown in figure 10. The nozzle was choked throughout the investigation; consequently, the manifold-loss total-pressure ratio $\bar{p}'_2/p'_1$ and the manifold energy loss are constant. The nozzle loss first increases and then decreases as the secondary flow rate is increased. The increase in loss is evidenced by the rapidly decreasing nozzle velocity coefficient (fig. 9) with increased secondary flow. At higher secondary flow rates, however, the nozzle velocity coefficient changes slowly while the nozzle pressure ratio $p'_1/\bar{p}_3$ continues to decrease, as evidenced by the rapid rise in nozzle-exit static pressure shown in figure 6(b). The combined effect of these changes is a decrease in nozzle loss.

The first-stage rotor loss (fig. 10) first decreases and then increases as a result of the corresponding changes in rotor velocity coefficient and pressure ratio. The first-stage rotor loss includes the work required to pump the secondary fluid into the flow stream and the loss resulting from leakage around the rotor shroud. The sum of these

TABLE I. - UTILIZATION OF AVAILABLE ENERGY

| Secondary flow, Y | Percent of ideal available energy, $\Delta h_s$ | | |
|---|---|---|---|
| | Work | Loss | Energy available to second stage |
| First stage | | | |
| 0 | 0.467 | 0.228 | 0.305 |
| .03 | .430 | .248 | .322 |
| .07 | .396 | .253 | .351 |
| .10 | .379 | .244 | .377 |
| Second stage | | | |
| 0 | 0.183 | 0.122 | ----- |
| .03 | .194 | .128 | ----- |
| .07 | .204 | .147 | ----- |
| .10 | .214 | .163 | ----- |

losses, which are quite small, is indicated by the dotted line (fig. 10). The maximum pumping loss was taken to be $YU_t^2/g_c J\theta_{cr}$ Btu per pound of primary flow.

The sum of the first-stage losses is almost constant over the range of secondary flow rates while the first-stage work decreases markedly. This condition results in an increase in energy available to the second stage and in increased second-stage work. The second-stage losses, however, also increase. The results presented in figure 10 are summarized in table I, where each parameter is related to the total turbine ideal available energy $\Delta h_s$.

The following observations are drawn from the table and from figure 10:

(1) At low secondary flow rates, decreased turbine work resulted from a marked increase in nozzle loss caused by off-design pressure ratio operation.

(2) As secondary flow rates were increased, first-stage losses remained essentially constant, whereas decreasing first-stage pressure ratio and increasing reaction resulted in less first-stage work and in increased energy available to the second stage.

(3) The increase in energy available to the second stage could not be fully utilized because the second-stage stator is essentially a turning vane and not a nozzle. Increased second-stage loss resulted in a further decrease in two-stage turbine work output at the higher secondary flow rates.

## SUMMARY OF RESULTS

The effect of injecting varying amounts of secondary flow into the space between the nozzle diaphragm and the first-stage rotor disk on the performance of a two-stage, velocity-compounded turbine designed for zero secondary flow was investigated experimentally. Performance data were taken for one and two-stage turbine configurations over a range of operating conditions and for four secondary flow rates of 0, 3, 7, and 10 percent of primary flow. The results of this investigation are as follows:

1. At design equivalent speed and pressure ratio, the two-stage turbine equivalent specific work decreased from 29.7 Btu per pound of primary flow at zero secondary flow to 27.0 Btu per pound of primary flow at a secondary flow rate of 10 percent of primary flow, with a corresponding decrease in static efficiency from 0.650 to 0.593.

2. Each increment of secondary flow resulted in substantial increases in interstage static pressures. The largest increase occurred at the exit of the converging-diverging nozzle. The reaction of the first stage increased markedly with each increment of secondary flow addition. This was also true, to a lesser extent, of the second stage. Both stages were forced farther from design operation as the secondary flow rate increased.

3. First-stage equivalent specific work decreased from 21.3 Btu per pound of primary flow at zero secondary flow to 17.3 Btu per pound of primary flow at a secondary flow rate of 10 percent of primary flow. First-stage losses were relatively constant over the range of secondary flow rates. The loss in work resulted primarily from decreased energy available to the first stage because of the pressure changes noted in result 2.

4. The energy available to the second stage increased with secondary flow rate. Some of this energy was converted to work. Second-stage equivalent specific work increased from 8.4 Btu per pound of primary flow at zero secondary flow to 9.7 Btu per pound at a secondary flow rate of 10 percent of primary flow. Second-stage losses, however, also increased, resulting in a further decrease in two-stage turbine work output as the secondary flow rate increased from 0 to 10 percent of primary flow.

Lewis Research Center,
National Aeronautics and Space Administration,
Cleveland, Ohio, December 5, 1966,
128-31-02-25-22.

## REFERENCES

1. Stabe, Roy G.; Kline, John F.; and Gibbs, Edward H.: Cold-Air Performance Evaluation of a Scale-Model Fuel Pump Turbine for the M-1 Hydrogen-Oxygen Rocket Engine. NASA TN D-3819, 1967.

2. Reynolds, T. W.: Aerodynamic Design - Model II Turbine M-1 Fuel Turbopump Assembly. Rep. No. AGC-8800-52(NASA CR-54820), Aerojet-General Corp., Apr. 15, 1966.

3. Ames Research Staff: Equations, Tables, and Charts for Compressible Flow. NACA TR 1135, 1953.

4. Keenan, Joseph H.; and Kaye, Joseph: Thermodynamic Properties of Air. John Wiley and Sons, Inc., 1945.